Seismic P-Velocities in Outcrops of the Troodos Ophiolite Complex, Cyprus

Report Prepared for Office of Naval Research

S. E. Dittus
J. R. Pelton

Center for Geophysical Investigation of the Shallow Subsurface
Boise State University
Boise, Idaho 83725

Technical Report BSU CGISS 97-04
15 September 1997

REPORT DOCUMENTATION PAGE

Form Approved
OMB No. 0704-0188

1. AGENCY USE ONLY *(Leave blank)*	2. REPORT DATE	3. REPORT TYPE AND DATES COVERED
	4/27/98	Final

4. TITLE AND SUBTITLE
Seismic P-Velocities in Outcrops of the Troodos Ophiolite

5. FUNDING NUMBERS
N00014-92-J-1143

6. AUTHOR(S)
Susan E. Dittus

7. PERFORMING ORGANIZATION NAMES(S) AND ADDRESS(ES)
CGISS
Boise State University
1910 University Drive
Boise, ID 83725

8. PERFORMING ORGANIZATION REPORT NUMBER

9. SPONSORING / MONITORING AGENCY NAMES(S) AND ADDRESS(ES)
ONR
800 N. Quincy St.
Arlington, VA 22217-5000

10. SPONSORING / MONITORING AGENCY REPORT NUMBER

11. SUPPLEMENTARY NOTES
CGISS Technical Report 97-04
15 September 1997

a. DISTRIBUTION / AVAILABILITY STATEMENT
Approved for public release; distribution unlimited

12. DISTRIBUTION CODE

13. ABSTRACT ***(Maximum 200 words)***

Estimates of seismic P-wave velocity for the rocks comprising the outcrops at the Troodos sites were obtained using three different procedures applied to the first arrival-time data:

1. *Straight-Ray Procedure*: computation of the reciprocal of the slope of a best-fit least-squares straight line through first arrival times plotted as a function of the distance along the straight ray from source to receiver;
2. *Hawkins' Procedure*: computation of the reciprocal of the slope of a best-fit least-squares straight line through corrected first arrival times plotted as a function of source-to-receiver offset (a procedure similar to that outlined by Hawkins, 1961, pp. 809-810);
3. *Ray-Tracing Procedure*: two-dimensional ray tracing inversion of first arrival times to determine a subsurface velocity model using the method of Zelt and Smith (1992).

For all three procedures, a simple subsurface velocity structure consisting of a near-surface low-velocity zone overlying higher velocity material was assumed at each site. This model corresponds to near-surface weathered zone overlying relatively unweathered bedrock. The major scientific use of the results of the velocity analyses is the comparison of the P-wave velocities of the unweathered bedrock to the lithological differences between the sites.

14. SUBJECT TERMS
Seismic P-velocities in basalt

15. NUMBER OF PAGES
40

16. PRICE CODE

17. SECURITY CLASSIFICATION OF REPORT	18. SECURITY CLASSIFICATION OF THIS PAGE	19. SECURITY CLASSIFICATION OF ABSTRACT	20. LIMITATION OF ABSTRACT
unclassified	unclassified	unclassified	

Seismic P-Velocities in Outcrops of the Troodos Ophiolite Complex, Cyprus

Report Prepared for Office of Naval Research

S. E. Dittus
J. R. Pelton

Center for Geophysical Investigation of the Shallow Subsurface
Boise State University
Boise, Idaho 83725

Technical Report BSU CGISS 97-04
15 September 1997

Table of Contents

Introduction

Three-component digital seismic refraction data were collected along profiles over outcrops of the Troodos Ophiolite Complex (Cyprus) as described by Dougherty et al. (1992). Estimates of seismic P-wave velocity for the rocks comprising the outcrops were obtained using three different procedures applied to the first arrival times:

1. *Straight-Ray Procedure*: computation of the reciprocal of the slope of a best-fit least-squares straight line through first arrival times plotted as a function of the distance along the straight ray from source to receiver;
2. *Hawkins' Procedure*: computation of the reciprocal of the slope of a best-fit least-squares straight line through corrected first arrival times plotted as a function of source-to-receiver offset (a procedure similar to that outlined by Hawkins, 1961, pp. 809-810);
3. *Ray-Tracing Inversion Procedure*: two-dimensional ray tracing inversion of first arrival times to determine a subsurface velocity model using the method of Zelt and Smith (1992).

For the second and third procedures, a simple subsurface velocity structure consisting of a near-surface low-velocity zone overlying higher velocity material was assumed at each site. This model corresponds to a near-surface weathered zone overlying relatively unweathered bedrock. The major scientific use of the results of the velocity analyses is the comparison of the P-wave velocities of the unweathered bedrock to the lithological differences between the sites. This report only addresses the velocity analyses and does not interpret the results in lithological terms.

Timing First Arrivals

The first stage of any interpretation of seismic data is the establishment of the arrival times for one or more wave types. The *first arrival time* is defined to be the time (measured from the shot initiation as time zero) of the first obvious break of the seismic trace from the background noise level. This first obvious break of the seismic trace corresponds to the arrival of the P-wave traveling between source and receiver along the fastest available path. Thus, the first arrival time is also commonly called the *P-wave travel-time*. Later arrivals, which may correspond to different wave types,

could not be clearly discerned in the Troodos data because of superposition of many different seismic signals.

Timing of first arrivals was performed using a MATLAB routine after transferring the Bison field records to a DECstation 5000 and converting them to MATLAB-readable format (MATLAB is a general-purpose computational program for scientists and engineers and is available from The Math Works, Natick, MA). The data were not corrected for phase delays associated with the seismic system; these delays were assumed to be uniform across the spread length for a given component.

To ensure consistency in measurement of the first arrival times, all the shot records for a particular site were analyzed by the same person working within an established system. The components (vertical, longitudinal, and transverse) for a given shot were analyzed separately. Irregularities in the data in the form of polarity reversals or the presence of precursors were noted. After analysis of a component for a particular shot record, the first arrival times were examined to identify anomalies. These anomalies were then checked for possible timing blunders and were corrected where appropriate.

Straight-Ray Procedure

Procedure

As a first step in the analysis of seismic velocity at a given Troodos site, a homogeneous and isotropic elastic subsurface was assumed so that a single number could be used to describe the P-wave velocity. A point source in a material of this type generates spherical wavefronts and straight rays, which in turn imply a linear graph of first arrival time plotted as a function of the distance along the straight ray from source to receiver. The reciprocal of the slope of the linear graph gives the seismic P-wave velocity of the subsurface.

Of course, real seismic field data will rarely be collected over a subsurface that closely approximates a homogeneous and isotropic elastic material with a single P-wave velocity. In the case of the Troodos seismic experiments, it is likely that there are at least two distinct P-wave velocities at each site, a relatively thin near-surface low-velocity layer representing weathered rock, and a region of faster velocity representing competent shallow bedrock. Since the near-offset geophones of the Troodos experiments may have recorded a P-wave propagating through the near-surface weathered layer, the first arrival times from near-offset geophones were discarded to better emphasize the P-wave velocity of the more competent shallow bedrock.

Computation of the distance along the straight ray between source and receiver was accomplished using the total station survey data and the usual formula for the distance between two points in space:

$$d = \sqrt{(x_R - x_S)^2 + (y_R - y_S)^2 + (z_R - z_S)^2} \qquad \text{(EQ 1)}$$

where d is the distance between source and receiver, and (x_S, y_S, z_S) and (x_R, y_R, z_R) are the rectangular coordinates of the source and receiver, respectively.

After the first arrival-time data were plotted as a function of distance between source and receiver, a best-fit straight line through the data was computed using the method of least squares. The reciprocal of the slope of this straight line constitutes an estimate of the P-wave velocity of the subsurface. Scatter about the best-fit straight line indicates random timing errors and residual shortcomings in the uniform velocity assumption. As an example, Figure 1 shows the results of a velocity determination at Site 1 for the longitudinal first arrival-time data of Shot 4.

For a given site, the straight-ray procedure was carried out separately for each component recorded during each shot. On center shots, velocity calculations were carried out in both directions. Thus, given a full complement of five shots at a site, and assuming a single seismic profile

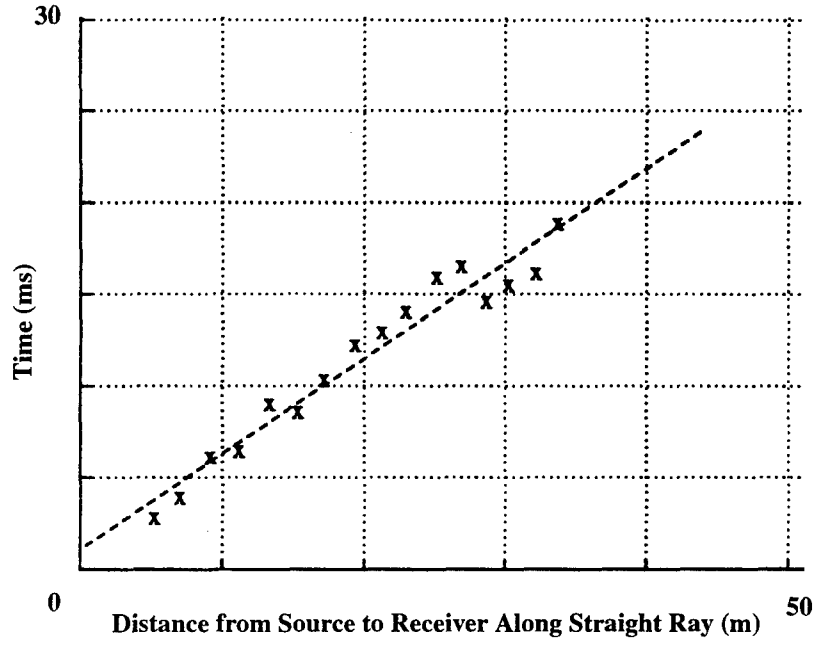

Figure 1. Example of velocity determination using first arrival times plotted as a function of the distance from source to receiver along a straight ray. The graph is for the longitudinal component of Shot 4 at Site 1. A velocity of 1925 m/s was calculated from the reciprocal of the slope of the best-fit least-squares straight line.

at the site, it is possible to compute six velocities for each geophone component and average the results.

Results

A summary of the P-velocity analysis by the straight-ray procedure is given in the table on the next page. Sites are arranged according to stratigraphic position (sites closest to the paleoseafloor given first) with the geographic location, type of alteration zone, gross lithology, and estimated depth below the paleoseafloor listed for each site (estimated depths below paleoseafloor from Gillis and Sapp, 1997; depths for sites 8-9, 11, and 12 are not known). At a given site, the mean velocity, estimated standard deviation of the mean velocity, and velocity range are given for each component, with the component with the largest mean velocity denoted by boldface print. Abbreviations used in the table are as follows: SFWZ-seafloor weathering zone; LTZ-low-temperature zone; V-vertical component; L-longitudinal component; T-transverse component.

Site	Alt Zone	Geographic Location Gross Lithology Depth Below Paleoseafloor	Cmp	Mean P-Vel (s. d.) (m/s)	No. Meas.	Velocity Range (m/s)
1	SFWZ	Akaki Canyon Pillow Lav2 0 m	V	2064 (116.3)	4	2299-1830
			L	2083 (97.2)	4	2291-1843
			T	**2102 (117.5)**	4	1817-1317
3	SFWZ	Akaki Canyon Pillow Lava 0 m	**V**	**2395 (84.0)**	**8**	2821-2085
			L	2326 (63.9)	8	2696-2093
			T	2205 (66.3)	8	2425-1906
2	SFWZ	Akaki Canyon Pillow Breccia 50 m	**V**	**1537 (146.3)**	**3**	1814-1317
			L	1534 (128.9)	3	1775-1274
			T	1468 (145.0)	3	1784-1170
6	LTZ	Margi Differentiated Massive Flow 50-100 m	**V**	**2813 (324.1)**	**6**	4391-2263
			L	2488 (62.8)	6	2781-2385
			T	2369 (121.2)	6	2930-2157
4	LTZ	Akaki Canyon Pillow Lava 200 m	**V**	**2471 (276.0)**	**5**	3995-1878
			L	2301 (366.2)	5	3710-1571
			T	2362 (387.8)	5	3829-1527
10	LTZ	Mathiati Mine Pillow Lava 300-400 m	**V**	**2208 (44.9)**	**4**	2309-2111
			L	2162 (44.2)	4	2294-2106
			T	2008 (86.3)	4	2136-1755
7	LTZ	Analiondas Pillow Lava 500 m	**V**	**3469 (267.9)**	**8**	4553-2666
			L	3254 (237.1)	8	4512-2573
			T	3154 (205.2)	8	4225-2607
5	LTZ	Eucalyptus Canyon Massive Flow 500 m	**V**	**2813 (626.8)**	**3**	4065-2120
			L	2580 (369.2)	3	3318-2191
			T	2642 (433.5)	3	3503-2127
8-9	LTZ	Kampia Mine Intercalated Hyaloclastites, Pillow Lavas, Sheet Flows, Sheeted Dikes ?? m	**V**	**2726 (229.8)**	**8**	4298-2265
			L	2551 (86.8)	8	2905-2210
			T	2422 (91.7)	8	2908-1956
11	LTZ	Delikipo Area Pillow Lavas Intermixed with Thin Sheet Flows ?? m	V	3019 (92.0)	6	3191-2584
			L	**3118 (64.7)**	**6**	3380-2905
			T	2689 (124.9)	6	3047-2163
12	LTZ	Peristerona River Series of Sheet Flows Underlain by Pillow Lavas ?? m	V	Straight-ray computations not carried out at Site 12. Single-component geophones were deployed in soil overlying bedrock.		
			L			
			T			

Examination of the standard deviations in the preceding table indicates that at a particular site, the differences between the mean velocity measured on the vertical component and the mean velocities measured on the horizontal components are not statistically significant. However, if one

examines the collection of all sites, the average vertical velocity is larger than the average horizontal velocities (longitudinal and transverse) at 8 of 10 sites (the only exceptions are Sites 1 and 11). This observation suggests statistical testing of the null hypothesis that there exists no bias towards measuring the maximum velocity on the vertical component. The formal statement of the null hypothesis is:

> H_0: $p = 1/3$ where p is the probability of measuring the maximum velocity on the vertical component,

In other words, H_0 states that in any given velocity determination, the maximum velocity is just as likely to be measured on any of the three components, so that the probability of measuring the maximum on the vertical component is one third. The appropriate test statistic is given by Pollard (1977, pp. 137-139):

$$T = \frac{(r - np_o)}{\sqrt{np_o(1 - p_o)}} \qquad \text{(EQ 2)}$$

where T is approximately distributed normally with zero mean and unit variance, $p_0 = 1/3$ (the probability of measuring the maximum velocity on the vertical component if there is no bias), r is the number of trials where the maximum velocity is measured on the vertical component ($r = 28$ in this case), and n is the total number of trials for the entire Troodos data set ($n = 55$ which is the number of shots recorded for which straight-ray velocities were determined using all three components). The value of T is 2.765 and standard tables for the unit normal distribution indicate that the probability of a larger value is less than 0.003. Thus, unless a rare outcome has occurred, the null hypothesis is rejected at a very high level of significance.

The outcome of the hypothesis test suggests that there is an overall tendency to time the first arrival on the vertical component earlier than on the horizontal components of the same geophone. Although this result was not confirmed by a rigorous check of the entire set of first arrival times, it is consistent with the general pattern noted during the timing stage of the data analysis. The sim-

plest explanation is a difference in system response between the horizontal and vertical components (i.e., a difference in phase delay between the vertical and horizontal components with the vertical component early). However, it is also possible that the particle velocity at the geophone during the first arrival may be oriented more vertically than horizontally, thereby giving a more impulsive signature on the vertical component that tends to be timed earlier.

The particle motion of first arrivals for the Troodos seismic experiments supports the conclusion that the first-arriving seismic energy involves particle velocities that are more vertical than horizontal. Specifically, 633 of 912 particle motion diagrams (69.4%) indicate an initial angle of particle velocity of 45^{o} or greater with the horizontal. Is the predominance (nearly 70%) of more vertically oriented particle velocity consistent with the basic assumption of P-waves propagating along straight rays? This question is not addressed in this report because it is complicated by the topography of the Troodos sites (see Appendix) and the partitioning of seismic energy at the free surface. Furthermore, rather than assuming straight rays, it may be more correct to view first-arriving seismic energy as following the path of a P-head wave generated at the base of the weathered layer and then returning to the surface at a steep angle. It is this latter possibility that is explored in the next sections (Hawkins' procedure and ray-tracing inversion procedure).

Hawkins' Procedure

Procedure

The term *Hawkins' procedure* refers here to a procedure for velocity determination that is associated with the reciprocal method of seismic refraction interpretation (Hawkins, 1961). The

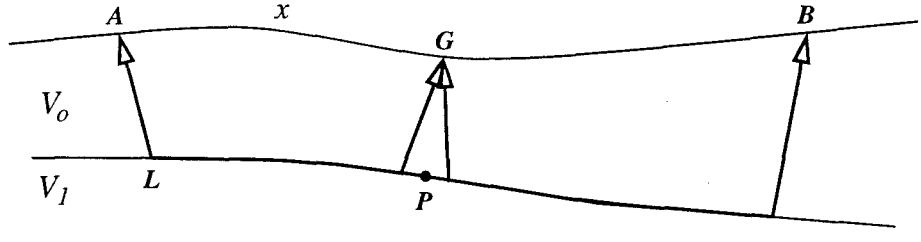

Figure 2. Subsurface model and rays used by Hawkins (1961) to develop the reciprocal method. Sources *A* and *B* are at the surface with receiver at *G*. Point *P* is the midpoint of the base of an isosceles triangle formed by the upgoing rays to *G*.

subsurface is assumed to consist of a near-surface low-velocity material (V_o) that overlies material of higher velocity (V_1) so that a head wave can be generated at the interface (Figure 2). Consider the reversed refraction profile from source *A* to source *B*, and visualize three head-wave rays:

- the ray from *A* to receiver *G*,
- the ray from *B* to receiver *G*, and
- the ray from source *A* to source *B*.

Now let t_{AG} be the travel time from *A* to *G*, let t_{BG} be the travel time from *B* to *G*, and let t_{AB} be the travel time from *A* to *B*. Using this notation, a new quantity, the *corrected travel time* (t'_{AG}), may be defined:

$$t'_{AG} = \frac{t_{AG} - t_{BG} + t_{AB}}{2} . \qquad \text{(EQ 3)}$$

The usefulness of t'_{AG} is that it may be shown to equal the travel time from *A* to *P* along the partial head-wave ray path *ALP* (Hawkins, 1961):

$$t'_{AG} = \frac{AL}{V_o} + \frac{LP}{V_1} \qquad \text{(EQ 4)}$$

To a first approximation, the distance along *LP* may be represented by the offset *x* measured along the surface between *A* and *G*:

$$t'_{AG} \approx \frac{AL}{V_o} + \frac{x}{V_1} \qquad \text{(EQ 5)}$$

Equation (5) indicates that t'_{AG} is a linear function of the offset *x* with slope $1/V_1$ and intercept AL/V_o. Thus, given the travel times required by equation (3) for a number of receiver positions between sources *A* and *B*, a plot of t'_{AG} as a function of offset *x* will yield a straight line whose slope can be inverted to give the velocity V_1 (i.e., the velocity of the material beneath the near-surface low-velocity layer).

The application of Hawkins' procedure to the Troodos seismic data requires that V_o be identified with the relatively thin near-surface low-velocity layer representing weathered rock, and V_1 be

identified with the underlying region of faster velocity representing competent shallow bedrock. Since each site had multiple pairs of shots to represent sources *A* and *B*, it was possible to repeat the t'_{AG} analysis several times for a given site and then compute a mean P-wave velocity for that site. Because the first arrival times tend to be earlier on the vertical component, the Hawkins' procedure was only applied to data recorded on the vertical components.

Results

A summary of the P-velocity analysis by the Hawkins' procedure is given in the table below. As in the previous velocity table, sites are arranged according to stratigraphic position (sites closest to the paleoseafloor given first) with the geographic location, type of alteration zone, gross lithology, and estimated depth below the paleoseafloor listed for each site (estimated depths below seafloor from Gillis and Sapp, 1997; depths for sites 8-9, 11, and 12 are not known). At a given site, the mean velocity and estimated standard deviation of the mean velocity are given for both the Hawkins' procedure and the straight-ray procedure; results from vertical component data only are shown. The larger of the two mean velocities at a given site is given in boldface print. Abbreviations: SFWZ-seafloor weathering zone; LTZ-low-temperature zone.

Site	Alt Zone	Site Location Gross Lithology Depth Below Paleoseafloor	Hawkins' Procedure Mean P-Vel (s. d.) No. Meas. (m/s)	Straight-Ray Proc. (Vert) Mean Vel (s. d.) No. Meas. (m/s)
1	SFWZ	Akaki Canyon Pillow Lava 0 m	**2090 (92.5)** 4	2064 (116.3) 4
3	SFWZ	Akaki Canyon Pillow Lava 0 m	**2420 (50.7)** 8	2395 (84.0) 8
2	SFWZ	Akaki Canyon Pillow Breccia 50 m	**1640 (140.2)** 2	1537 (146.3) 3
6	LTZ	Margi Differentiated Massive Flow 50-100 m	2610 (63.2) 6	**2813 (324.1)** **6**

Site	Alt Zone	Site Location Gross Lithology Depth Below Paleoseafloor	Hawkins' Procedure Mean P-Vel (s. d.) No. Meas. (m/s)	Straight-Ray Proc. (Vert) Mean Vel (s. d.) No. Meas. (m/s)
4	LTZ	Akaki Canyon Pillow Lava 200 m	**2780 (115.5)** 2	2471 (276.0) 5
10	LTZ	Mathiati Mine Pillow Lava 300-400 m	2180 (67.6) 4	**2208 (44.9)** 4
7	LTZ	Analiondas Pillow Lava 500 m	3120 (56.5) 8	**3469 (267.9)** 8
5	LTZ	Eucalyptus Canyon Massive Flow 500 m	2480 (134.9) 2	**2813 (626.8)** 3
8-9	LTZ	Kampia Mine Intercalated Hyaloclastites, Pillow Lavas, Sheet Flows, and Sheeted Dikes ?? m	2510 (49.2) 8	**2726 (229.8)** 8
11	LTZ	Delikipo Area Pillow Lavas Intermixed with Thin Sheet Flows ?? m	**3030 (83.8)** 8	3019 (92.0) 6
12	LTZ	Peristerona River Series of Sheet Flows Underlain by Pillow Lavas ?? m	2240 (62.9) 4 2790 (83.5) 4	Straight-ray computations not carried out at Site 12. Single-component geophones were deployed in soil overlying bedrock.

Comparison of results from the straight-ray and Hawkins' procedures indicates reasonable consistency in P-wave velocity determinations. This statement is strengthened if one considers the estimated standard deviations of the mean velocities. There is no overall tendency for mean velocity estimates to be higher for the Hawkins' procedure (i.e., the boldface velocities occur 5 times in the Hawkins' column and 5 times in the straight-ray column).

Ray-Tracing Inversion Procedure

Ray tracing may be combined with modern inversion theory to provide a powerful velocity estimation technique. In this technique, observed first arrival times are compared with theoretical times computed according to geometrical ray theory applied to a realistic subsurface velocity

model. The initial model is systematically modified until the fit between the observed and theoretical travel times meets some predetermined criteria.

Ray-tracing inversion of the Troodos seismic data was accomplished using RAYINVR, a public domain program developed at the University of Utah (Zelt and Smith, 1992) and based on a fast raytracing algorith developed at the University of British Columbia (Zelt and Ellis, 1988). A fundamental feature of RAYINVR is its two-dimensional, layered, variable-sized block parameterization which allows for both efficient ray tracing and a minimum number of independent model parameters. Although RAYINVR was developed for use on crustal seismic data (scale of profiles measured in hundreds of km), the program is very flexible and can be used effectively for outcrop seismic data (scale of profiles less than 100 m). The theory and methodology on which RAYINVR is based are described by Zelt and Smith (1992).

Methodology for Ray Tracing

The model is parameterized as a sequence of layers, and each layer is comprised of a series of adjacent trapezoids with vertical sides. Velocities may be continuous or discontinuous across layer boundaries but are continuous laterally within a given layer. Layers may be reduced to zero thickness so that pinchouts and bodies of finite lateral dimension can be modeled. In order to minimize scattering and focusing of rays associated with refraction at layer boundaries (which consist of straight line segments), RAYINVR includes an option that simulates smooth layer boundaries.

Raytracing within a layer is carried out by solving one of the following sets of equations using a Runge-Kutta method:

$$\frac{dz}{dx} = \cot\theta \qquad \frac{d\theta}{dx} = \frac{(v_z - v_x \cdot \cot\theta)}{v} \qquad \text{(for near horizontal ray paths)} \qquad \text{(EQ 6)}$$

$$\frac{dx}{dz} = \cot\theta \qquad \frac{d\theta}{dz} = \frac{(v_z \cdot \tan\theta - v_x)}{v} \qquad \text{(for near vertical ray paths)} \qquad \text{(EQ 7)}$$

where x and z are the horizontal and vertical rectangular coordinates, respectively, θ is the angle between the tangent to the ray and the z-axis, v is the wave velocity at point (x, z), and the partial derivatives of v with respect to x and z are given by v_x and v_z, respectively. The initial conditions require that the starting point (x_0, z_0) and take-off angle (θ_0) of the ray be specified. Ray step lengths (increments in either the x or z directions) are automatically determined to improve efficiency without sacrificing accuracy. Snell's law is applied at the intersection of a ray with a layer boundary. Rays may be traced that correspond to turning waves, reflected waves, and head waves.

Methodology for Inversion

The formulation of P-wave travel-time inversion as implemented by RAYINVR begins with the following assumptions:

- the propagation of P-waves through the subsurface is accurately represented by zero-order asymptotic ray theory in a two-dimensional velocity model;
- the two-dimensional velocity model can be adequately described by M model parameters, where M is a finite number.

Suppose we have N measured P-wave travel-times from a given seismic experiment. If t_i represents the theoretical travel time for source-receiver pair i, then the assumptions listed above imply that t_i is a function of M model parameters (denoted in this report by $m_1, m_2, ..., m_M$), and that t_i will equal the observed travel time when the model parameters take on their "true" values (the parameters that represent the actual subsurface). Now let $\eta_1, \eta_2, ..., \eta_M$ be the "true" model parameters, and let $\mu_1, \mu_2, ..., \mu_M$ be the "trial" model parameters (any parameters other than the true parameters). Using these definitions, the observed travel time at station i can be expressed as a Taylor series expansion of t_i about the trial model parameters:

$$t_i(\eta_1, \eta_2, \ldots, \eta_M) = t_i(\mu_1, \mu_2, \ldots, \mu_M) + \sum_{j=1}^{M} (\eta_j - \mu_j) \left. \frac{\partial t_i}{\partial m_j} \right|_{m_k = \mu_k} + O \qquad \text{(EQ 9)}$$

where O represents higher order terms and $i = 1, 2, ..., N$. If the trial model is sufficiently close to

the true model, then the higher order terms may be neglected and equation (9) can be rewritten in linearized form as follows:

$$\Delta t_i = \sum_{j=1}^{M} \Delta m_j \left. \frac{\partial t_i}{\partial m_j} \right|_{m_k = \mu_k} \qquad i = 1, 2, \ldots, N \qquad \text{(EQ 10)}$$

where $\Delta m_j = (\eta_j - \mu_j)$ is the *parameter correction vector* and Δt_i is the *travel-time residual* given by:

$$\Delta t_i = t_i(\eta_1, \eta_2, \ldots, \eta_M) - t_i(\mu_1, \mu_2, \ldots, \mu_M) \qquad i = 1, 2, \ldots, N \qquad \text{(EQ 11)}$$

The matrix version of equation (10) is:

$$\Delta \mathbf{t} = \mathbf{A}\Delta\mathbf{m} \qquad \text{(EQ 12)}$$

where **A** is the N x M matrix of partial derivatives. The model parameters used by RAYINVR are the z-coordinates of special points on each surface between layers (i.e., *boundary nodes*) and the P-wave velocities at special points at the top and bottom of each layer (i.e., *velocity nodes*).

The solution of equation (12) for $\Delta\mathbf{m}$ is a discrete inverse problem (see Menke, 1989, for a popular monograph on discrete inverse theory). A basic feature of this problem is that it is common for some model parameters to be overdetermined and some to be underdetermined. Under these conditions, the methods of discrete inverse theory define the solution vector (denoted by $\Delta\mathbf{m}_\mathbf{s}$) to be the parameter correction vector that simultaneously minimizes the norm of the *prediction error*

$$\left\| \Delta\mathbf{t} - \mathbf{A}\Delta\mathbf{m}_\mathbf{s} \right\| \qquad \text{(EQ 13)}$$

plus the norm of the parameter correction vector (i.e., the *solution length*):

$$\left\| \Delta\mathbf{m}_\mathbf{s}^\mathbf{T} \Delta\mathbf{m}_\mathbf{s} \right\|. \qquad \text{(EQ 14)}$$

If the L_2 norm is selected, then simultaneous minimization of (13) plus (14) yields the damped least-squares solution:

$$\Delta\mathbf{m}_\mathbf{s} = (\mathbf{A}^\mathbf{T}\mathbf{C}_t^{-\mathbf{1}}\mathbf{A} + D\mathbf{C}_m^{-\mathbf{1}})^{-1}\mathbf{A}^\mathbf{T}\mathbf{C}_t^{-\mathbf{1}}\Delta\mathbf{t} \qquad \text{(EQ 15)}$$

where D is the damping factor (determines the trade-off between minimizing prediction error and solution length), $\mathbf{C}_t$ and $\mathbf{C}_m$ are the estimated data and model covariance matrices, respectively,

$$\mathbf{C}_t = diag\{\sigma_i^2\} \qquad \mathbf{C}_m = diag\{\sigma_j^2\}, \tag{EQ 16}$$

and where σ_i is the estimated uncertainty of t_i (considering equipment limitations and human error in timing first arrivals) and σ_j is an *a priori* estimate of uncertainty of parameter m_j. The inverses of $\mathbf{C}_t$ and $\mathbf{C}_m$ in (15) serve as weighting matrices so that some observations and model parameters can be emphasized. The text by Menke (1989) and the paper by Zelt and Smith (1992) may be consulted for details on the damped least squares method, including the question of the trade-off between resolution and variance.

Ray-tracing inversion of travel times is nonlinear in the sense that the higher order terms in equation (9) cannot be neglected in general. The standard practice is to choose a reasonable set of *initial trial parameters* and then solve the nonlinear inversion by successive linear iterations. A formulation of the basic inversion procedure is as follows:

1. Estimate the uncertainties σ_i and σ_j and create the covariance matrices (equation 16).
2. Choose initial trial model parameters $\mu_1, \mu_2, ..., \mu_M$.
3. Compute $\Delta\mathbf{t}$ using equation (11).
4. Compute the matrix of partial derivatives $\mathbf{A}$ evaluated at $\mu_1, \mu_2, ..., \mu_M$ (the method used in RAYINVR is described by Zelt and Smith, 1992).
5. Compute $\Delta\mathbf{m}_s$ according to damped least-squares (equation 15) with a damping parameter typically chosen between 1-10.
6. Add $\Delta\mathbf{m}_s$ to the initial trial model parameters to obtain a new trial model.
7. Repeat steps 3-6 until the root-mean-square (RMS) travel-time residual is within specified limits.

Initial RAYINVR Trial Model

The upper or ground surface of the initial RAYINVR trial model for a given Troodos site was defined by total station topographic survey data (Dougherty et al., 1992). One additional surface was defined at a constant depth beneath the ground surface. This additional surface was intended to represent a weathered layer overlying a layer of competent bedrock. Results from the straight-ray and Hawkins' procedures (see preceding tables) were used to determine initial trial velocity parameters. Minor adjustments were made until a reasonable fit of observed to calculated travel times was achieved. At this point, the initial trial model was declared ready for an inversion by the damped least squares method outlined above. Figure 3 shows an example of a RAYINVR initial trial model for Site 8 at Kampia mine.

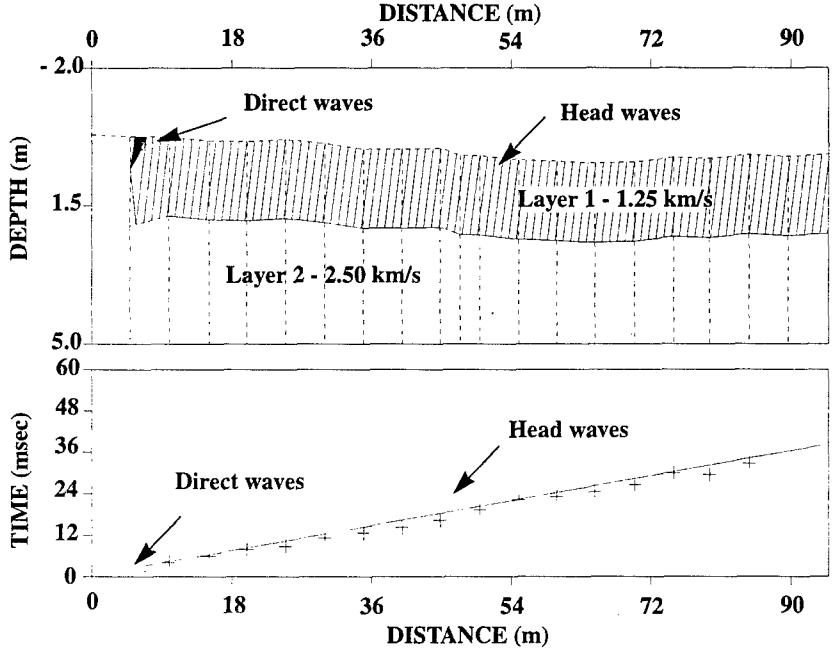

Figure 3. Initial trial model for Site 8, located on the north face of Kampia mine. The upper portion of the diagram illustrates the initial trial model, with ray paths for direct waves and head waves also shown. Dashed lines indicate the vertical boundaries of the model blocks. Initial trial velocity and depth values are entered for each corner of these blocks. The lower plot shows the observed first arrival times as crosses with the calculated first arrival times as solid lines. The first layer is uniformly 2-m thick for the entire line, with a uniform velocity of 1.25 km/s. Velocity of the second layer, 2.50 km/s, was taken directly from results of the Hawkins' procedure. This initial trial model fits the data reasonably well, with calculated times being slightly greater than real times. Only the ray paths for one shot are shown here, whereas in the inversion all shots at Site 8 are considered.

Inversion

The RAYINVR inversion of P-wave travel time data at a particular site involve changes in depth of the boundary nodes, changes in P-velocity at the velocity nodes, or simultaneous changes in both (Figures 4-6). Changes must not violate known geology or the measured topography;

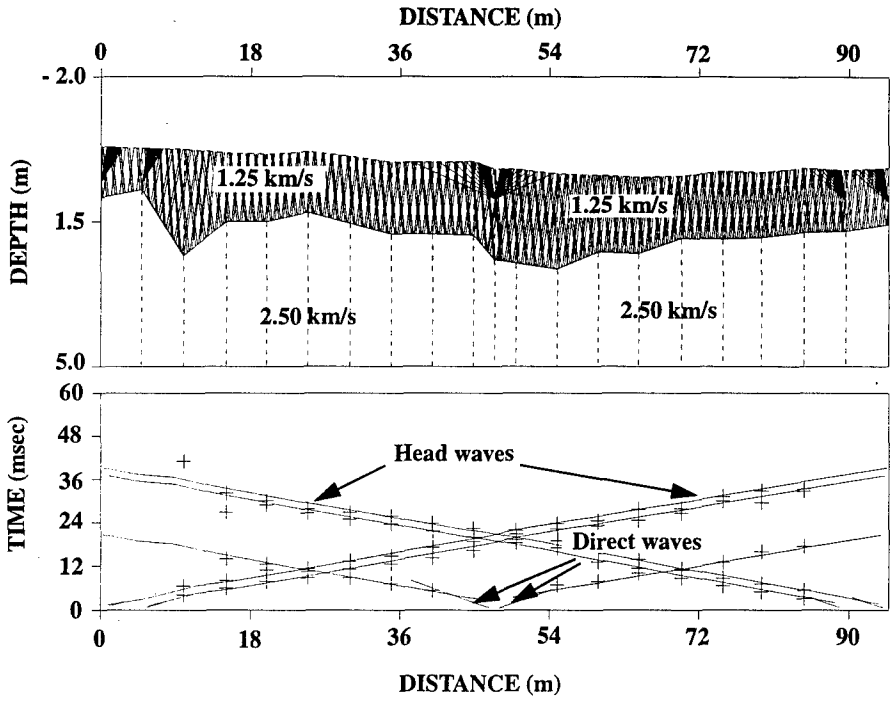

Figure 4. Depth variant inversion of the initial model shown in Figure 3 for Site 8. All velocities are kept constant. Note that there are now two distinct depressions in the upper layer.

unwanted changes can be controlled by a RAYINVR option that permits fixed values at boundary and velocity nodes. Maximum changes in depth and velocity per iteration were set at 0.05 m and 0.05 km/s, respectively. As RAYINVR converges on a solution, some of the observed first arrival times will be discarded by the program if they cannot be reasonably incorporated into the inversion.

The final inversions indicate that a low velocity layer is present at the surface at all the Troodos sites. Models without a surficial low-velocity layer failed to match the arrival times satisfactorily and often introduced unreasonable velocities or changes in layer thickness that could not be reconciled with the outcrop geology. The low velocity layer probably represents the surficial weathering zone noted by Gillis and Sapp (1997) at the Troodos sites. At two sites (6 and 12), attempts to use

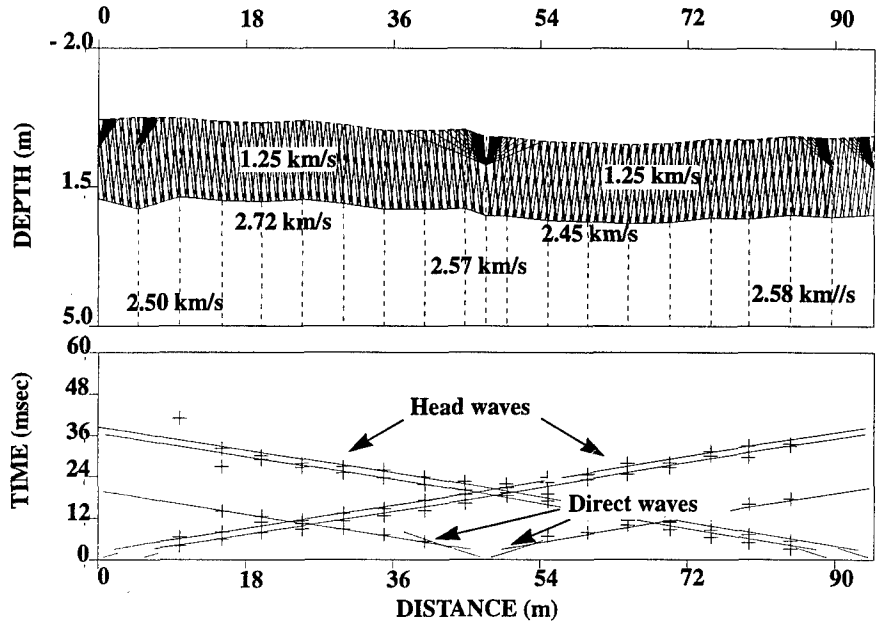

Figure 5. Velocity variant inversion of the initial model shown in Figure 3 for Site 8. In this case the velocity and thickness of the upper layer was kept constant. The velocity values increased during the inversion, with only one area of decrease near 54 m (the same position where upper layer thickness increased in Figure 4).

a two-layer model repeatedly failed, but once a third layer was introduced the inversion produced a very close match to the observed travel times. In each case the introduction of a third layer makes geological sense (at Site 6, the middle layer appears to represent the colonnade at the site, overlain by less competent rock; at Site 12, the layers represent overburden, weathered rock, and more competent rock). All other sites were modeled using two velocity layers.

There is an inherent weakness in the final RAYINVR models. At each site, the velocity of the first layer is based on only a few direct arrivals. Trade-offs exist between the thickness of the first layer and its velocity. Slow velocities will result in a thinner first layer, and faster velocities in a thicker first layer. The mapped outcrop geology is the best check on whether the first layer properties are reasonable. Even so, in many areas the geologic information has limitations, and the thickness and velocity of the first layer is open to question at many sites.

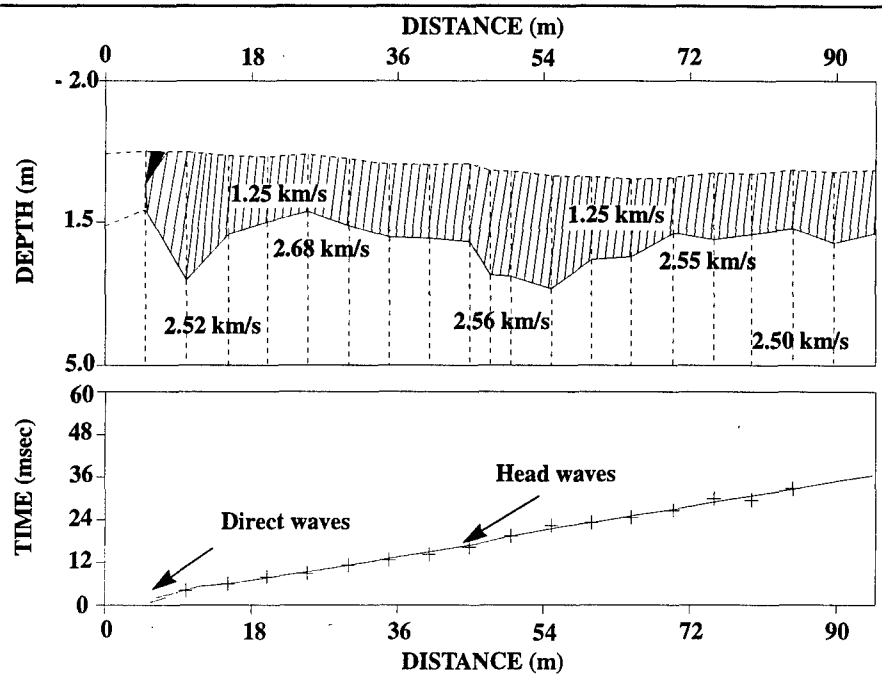

Figure 6. Combination inversion with variations in depth and velocity of the initial model shown in Figure 3 for Site 8. For clarity, only rays from one shot are shown. The changes in the thickness of the low velocity layer are as in the depth inversion (Figure 4), while the velocity changes in the second layer are more subdued than in the velocity inversion. The depth changes are reasonable when the geology of the site is taken into consideration, so this inversion can be viewed as an acceptable interpretation of the seismic data for this site.

Final Models

The final RAYINVR models for the Troodos sites are shown in the Appendix. All length scales are in meters (m), and all time scales are in milliseconds (ms). Velocities at different points in the final models are given in kilometers per second (km/s).

References

Dougherty, Martin E., Gillis, Kathryn M., and John R. Pelton, Heterogeneity and permeability structure of the upper oceanic crust, Troodos Ophiolite Complex, Cyprus, May-June 1992 Field Report, *Technical Report 92-05*, Center for Geophysical Investigation of the Shallow Subsurface (CGISS), Boise State University, Boise, ID, 72 pp., 1992.

Gillis, Kathryn M., and Kimberly Sapp, Distribution of porosity in a section of upper oceanic crust exposed in the Troodos Ophiolite, *Journal of Geophysical Research*, 102, 10,133-10,149, 1997.

Hawkins, L. V., The reciprocal method of routine shallow seismic refraction investigations, *Geophysics*, 26, 806-819, 1961.

Menke, William, Geophysical data analysis: discrete inverse theory, International Geophysics Series (Vol. 45), Academic Press, San Diego, CA, 289 pp., 1989.

Pollard, J. H., A handbook of numerical and statistical techniques, Cambridge University Press, Cambridge, 349 pp., 1977.

Zelt, C. A., and R. M. Ellis, Practical and efficient ray tracing in two-dimensional media for rapid traveltime and amplitude forward modeling, *Canadian Journal of Exploration Geophysics*, 24, 16-31, 1988.

Zelt, C. A., and R. B. Smith, Seismic traveltime inversion for 2-D crustal velocity structure, *Geophys. J. Int.*, 108, 16-34, 1992.

Appendix

Final RAYINVR Models

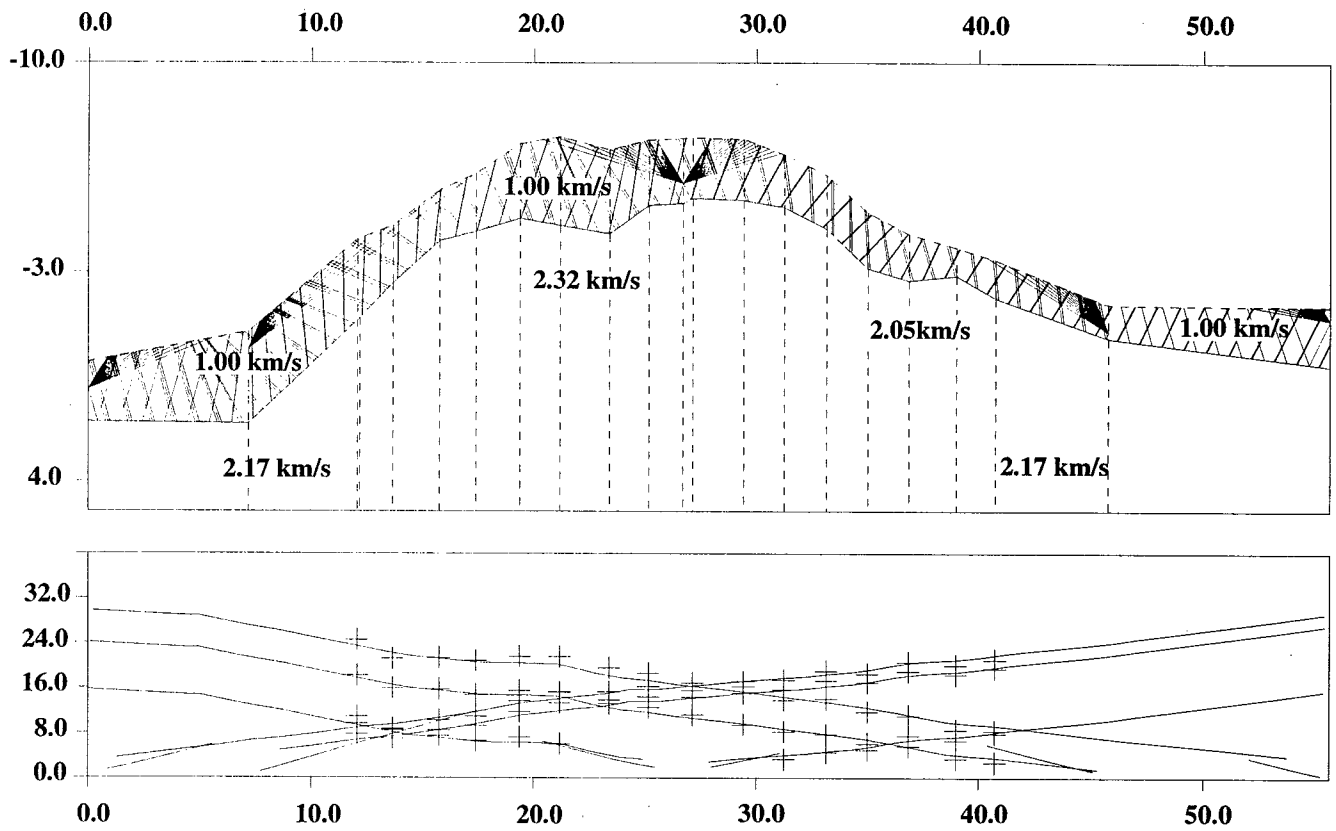

Site 1 RAYINVR

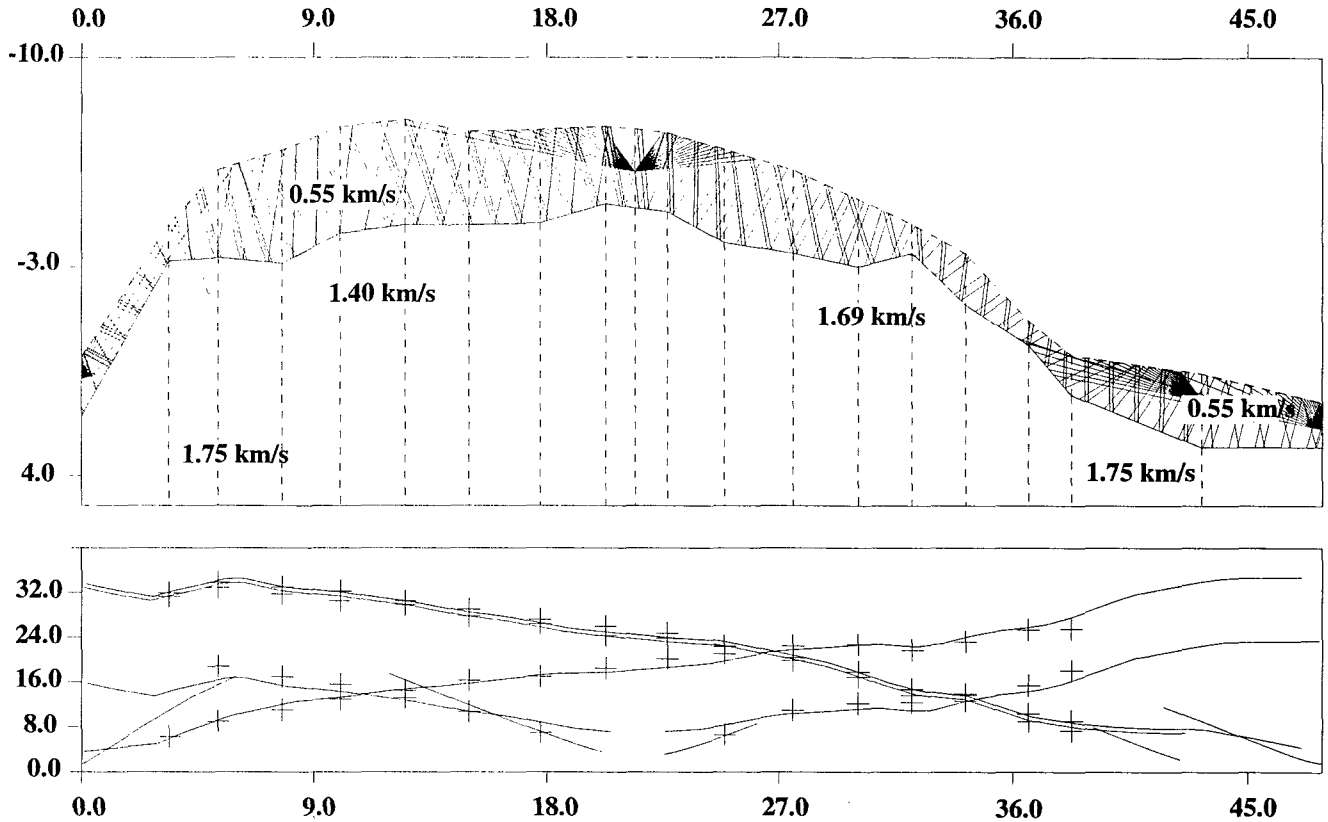

Site 2 RAYINVR

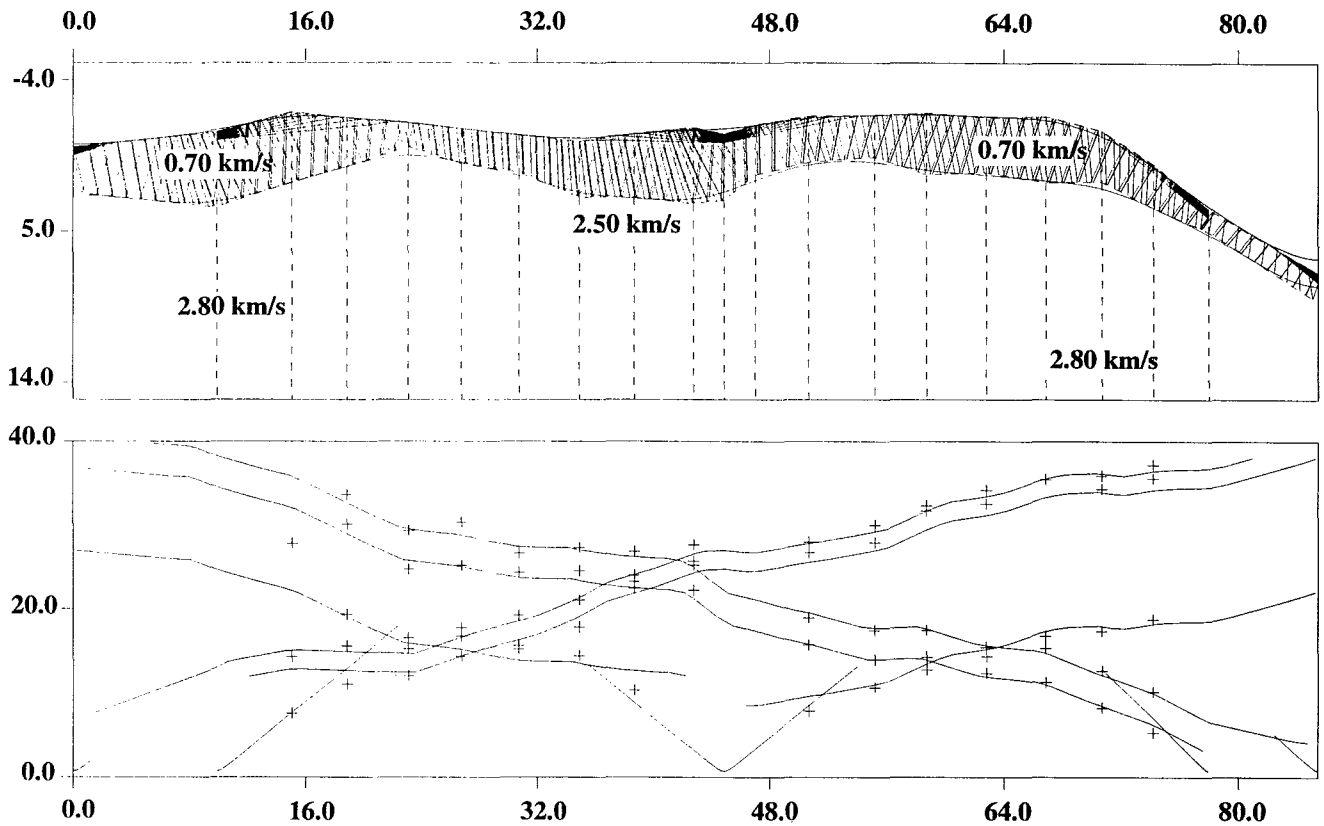

Site 3l RAYINVR

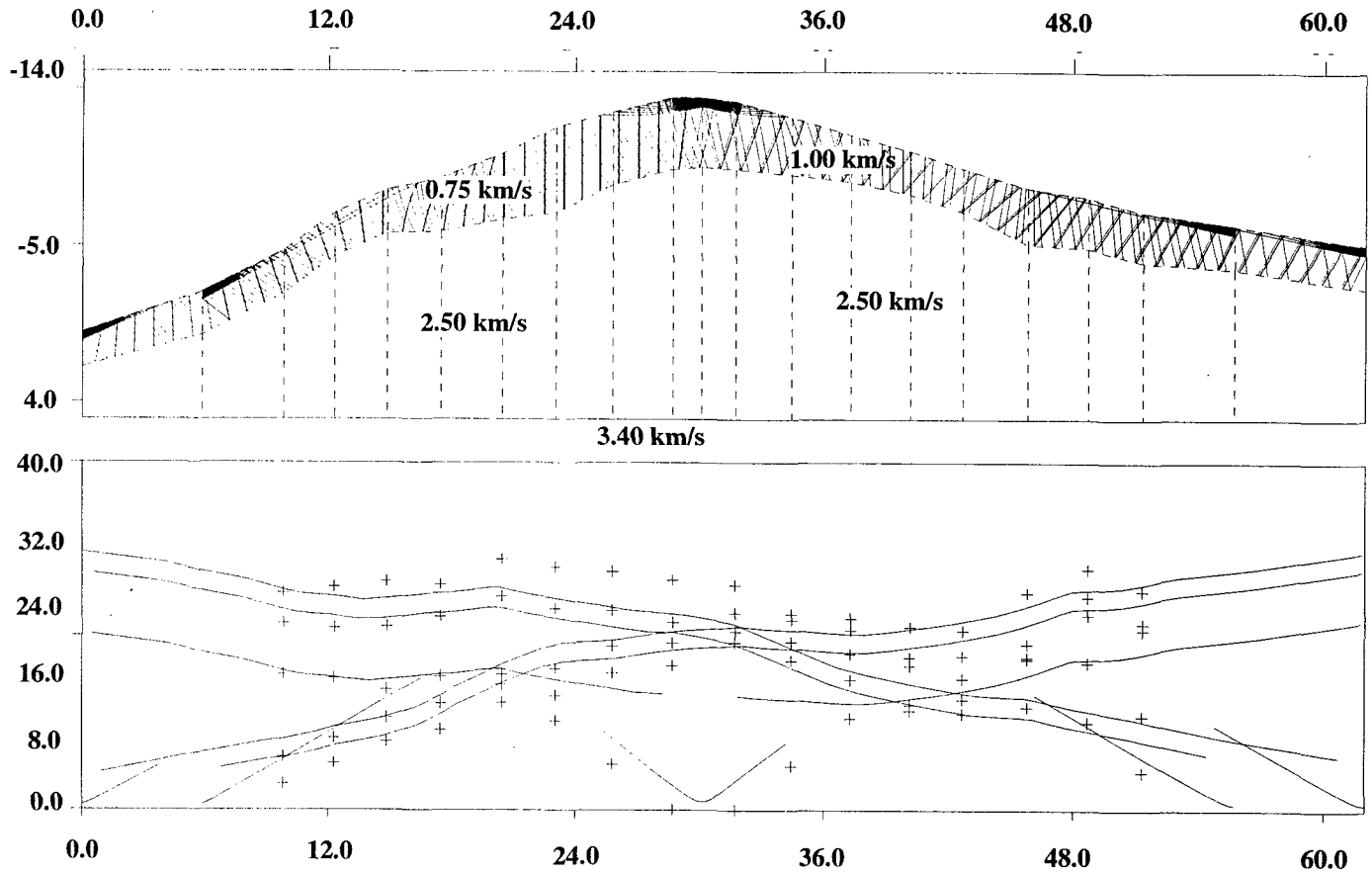

Site 3c RAYINVR

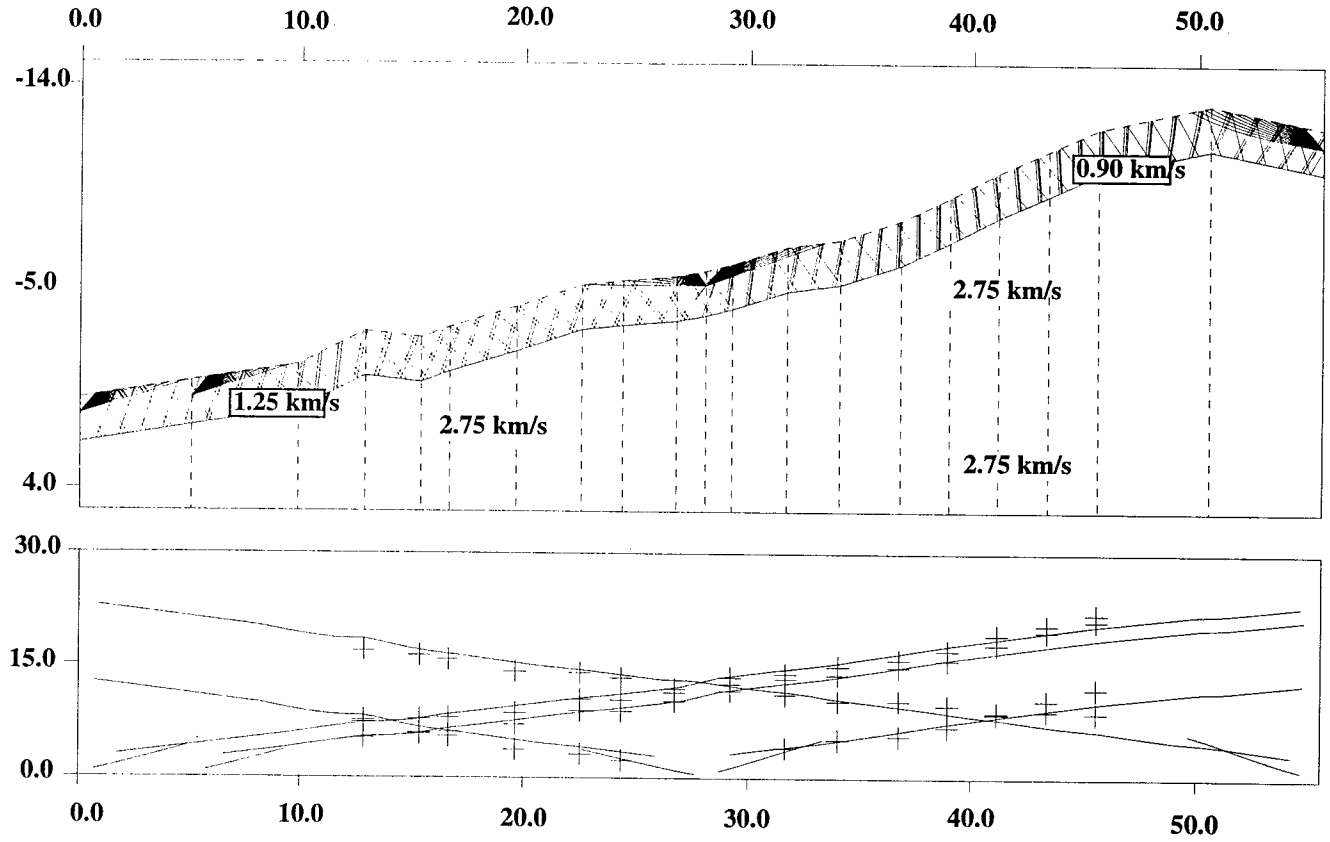

Site 4 RAYINVR

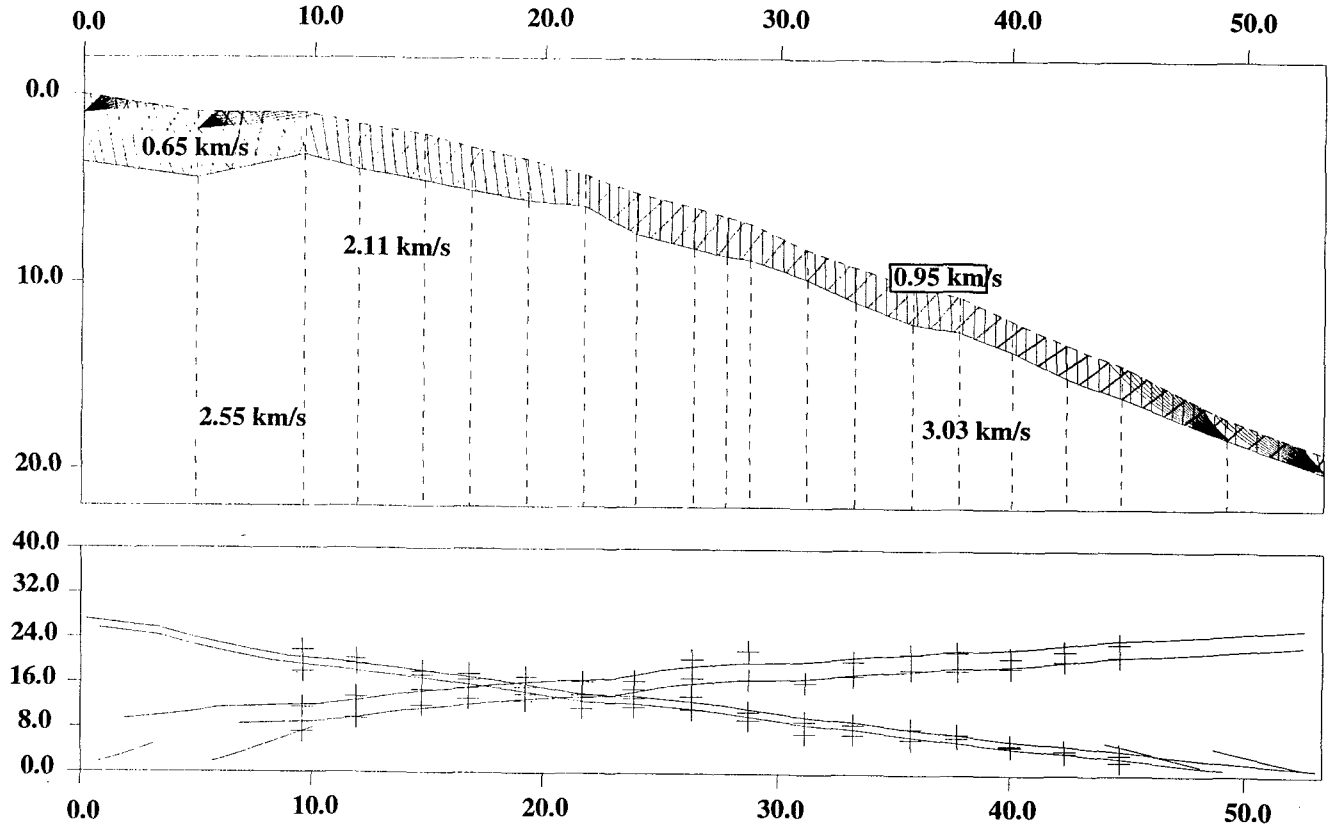

Site 5 RAYINVR

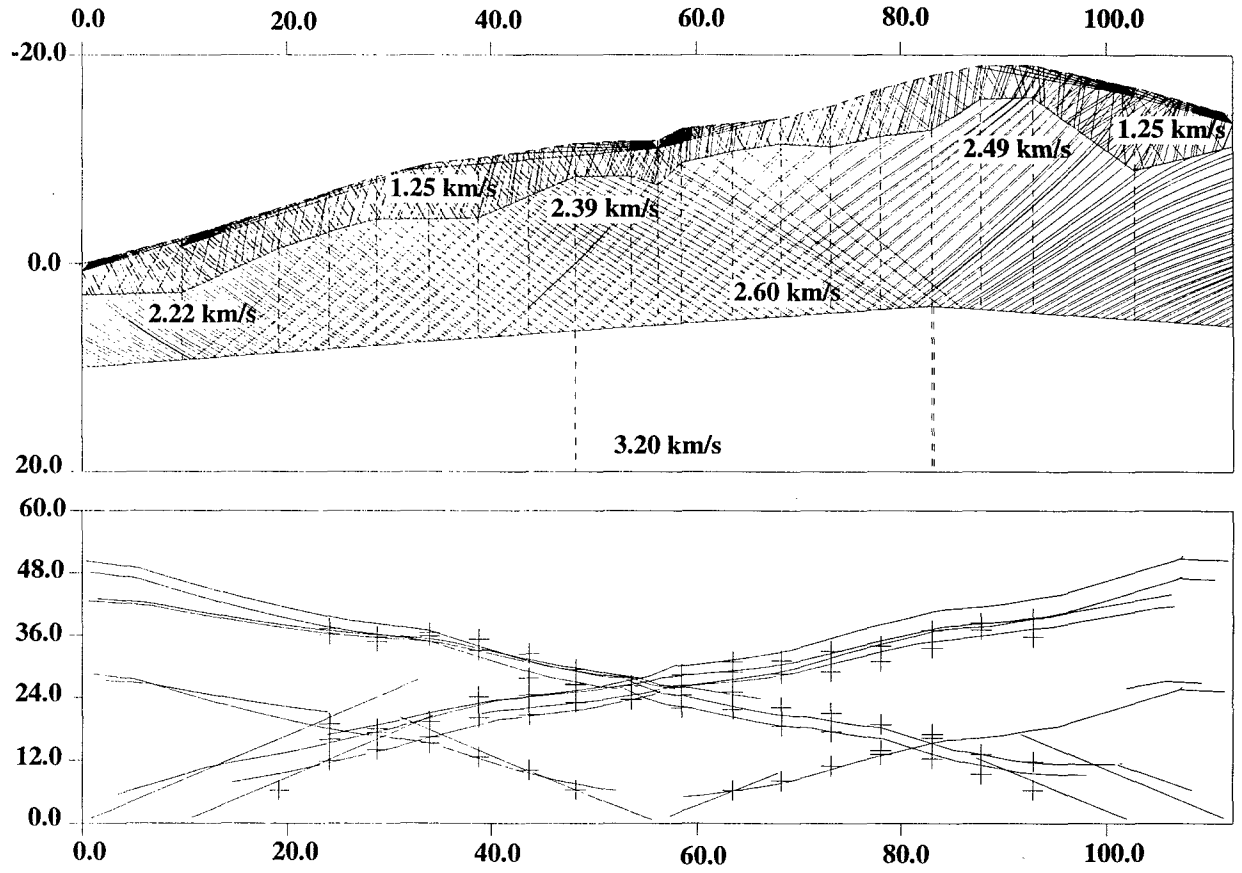

Site 6l RAYINVR

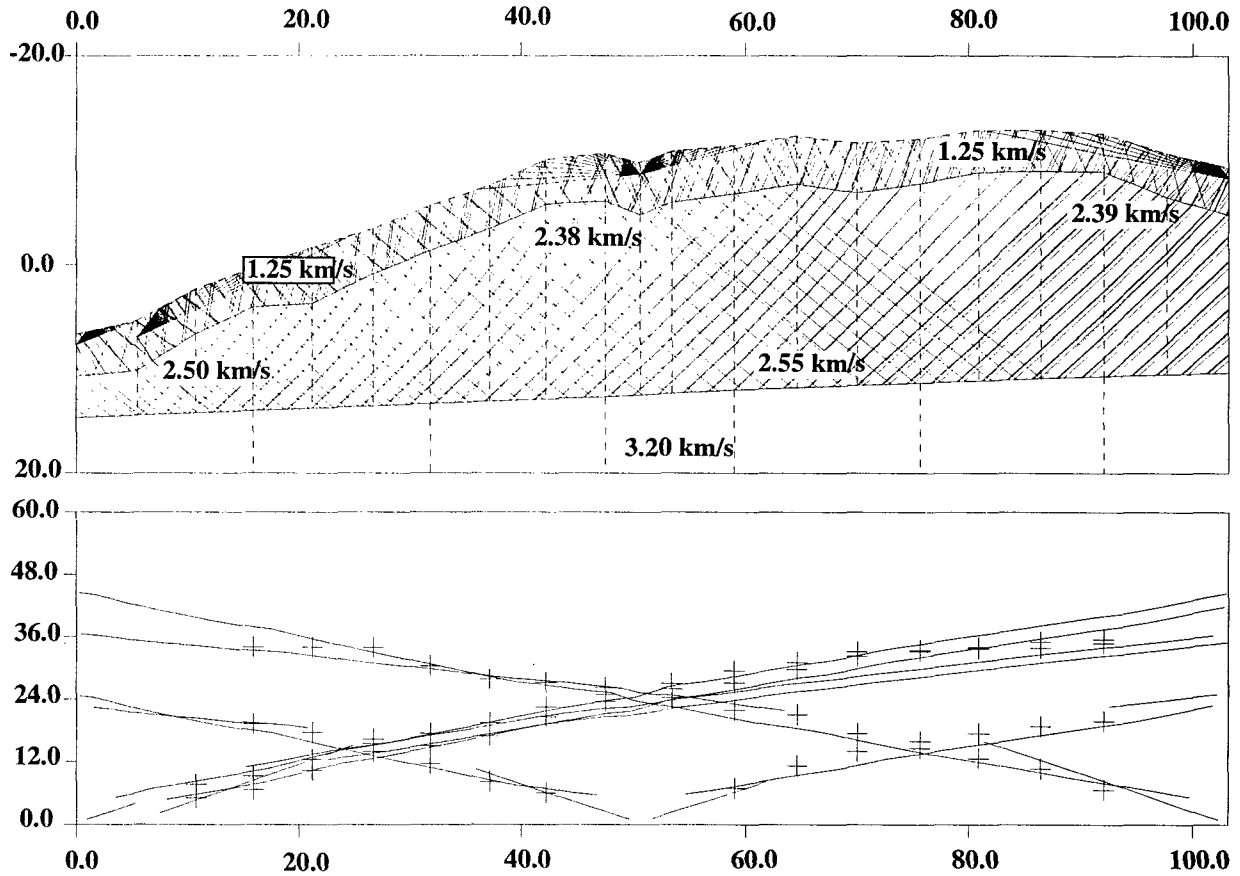

Site 6u RAYINVR

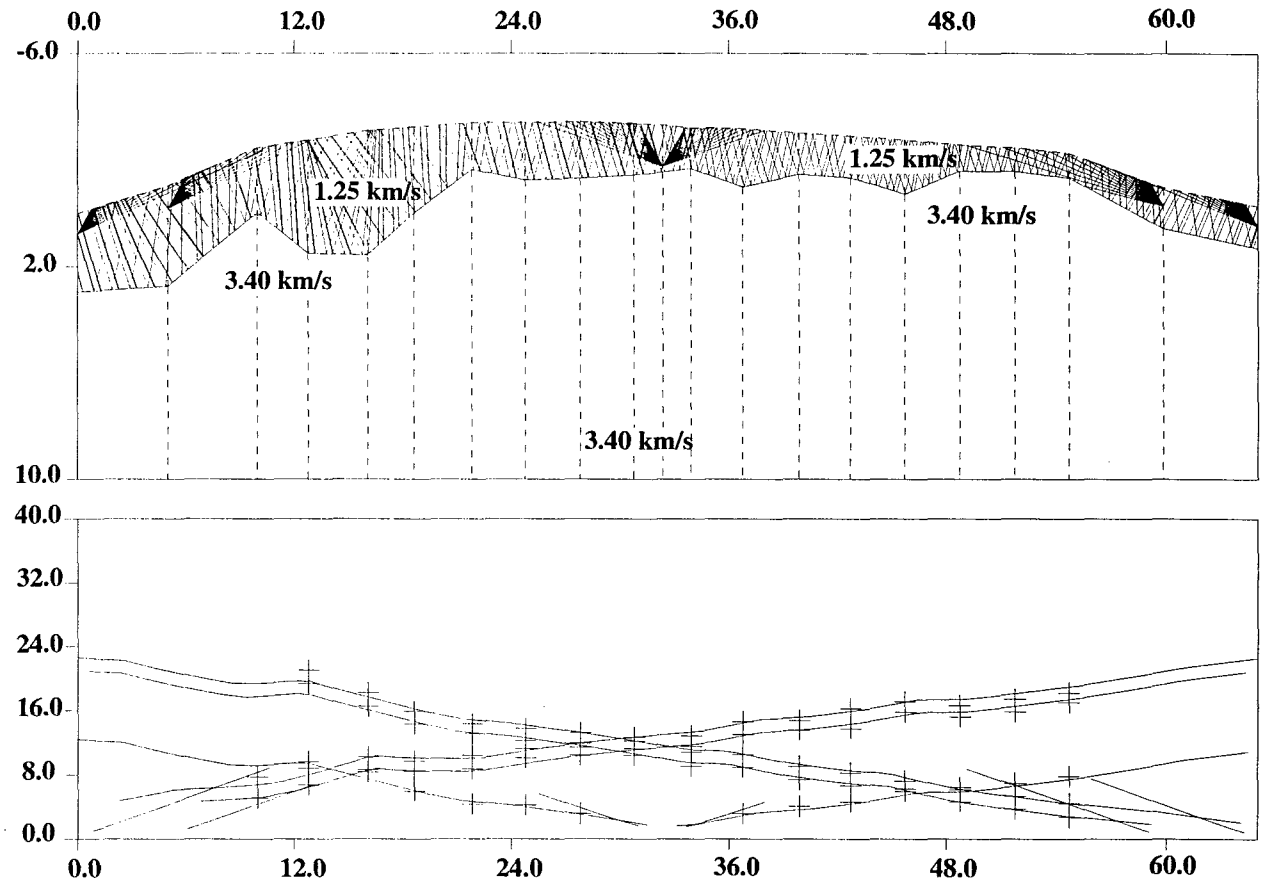

Site 7l RAYINVR

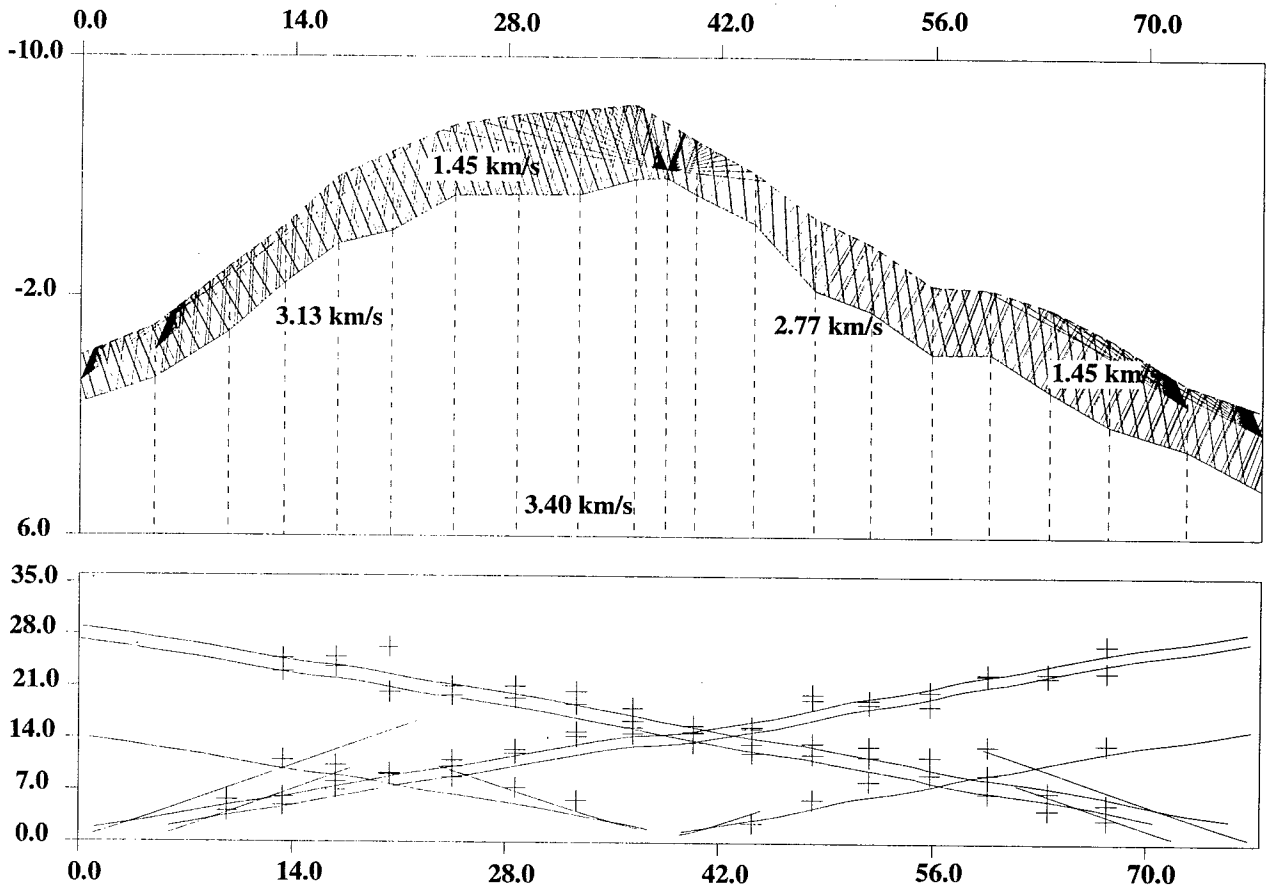

Site 7u RAYINVR

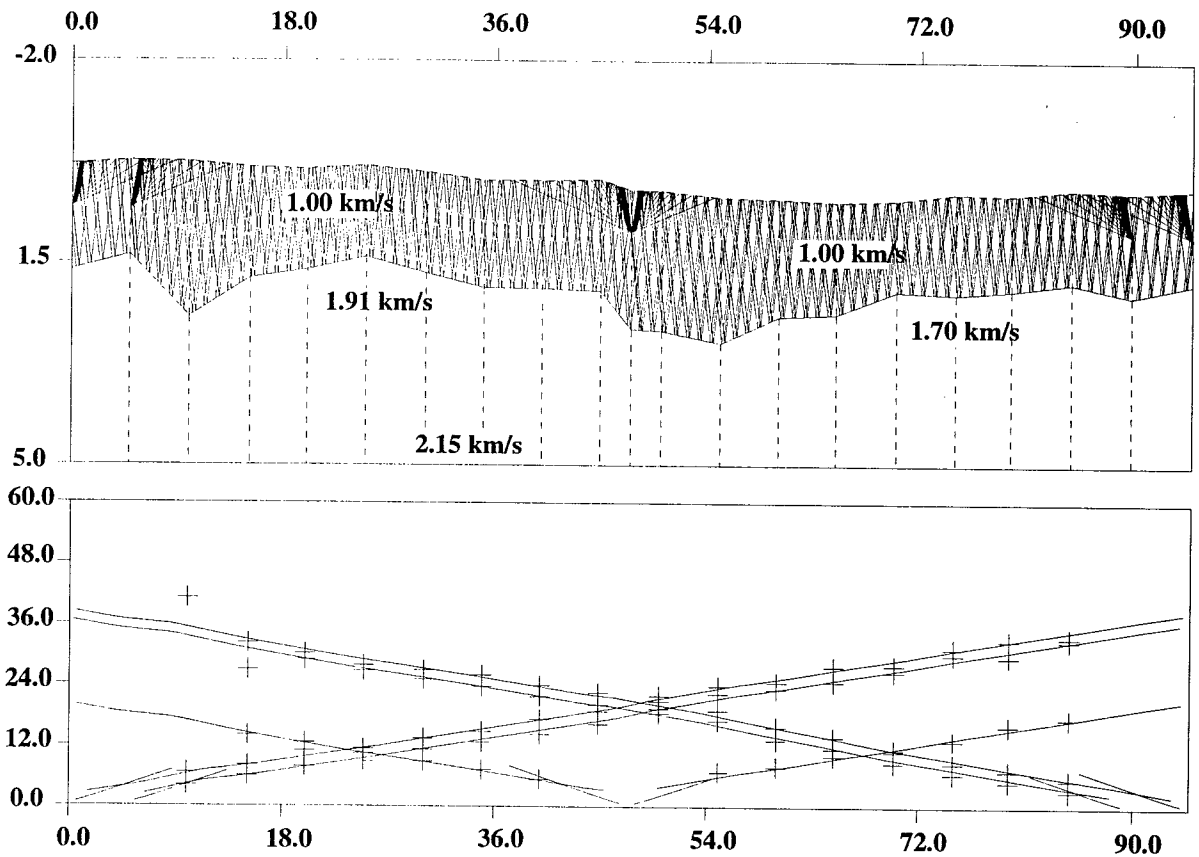

Site 8 RAYINVR

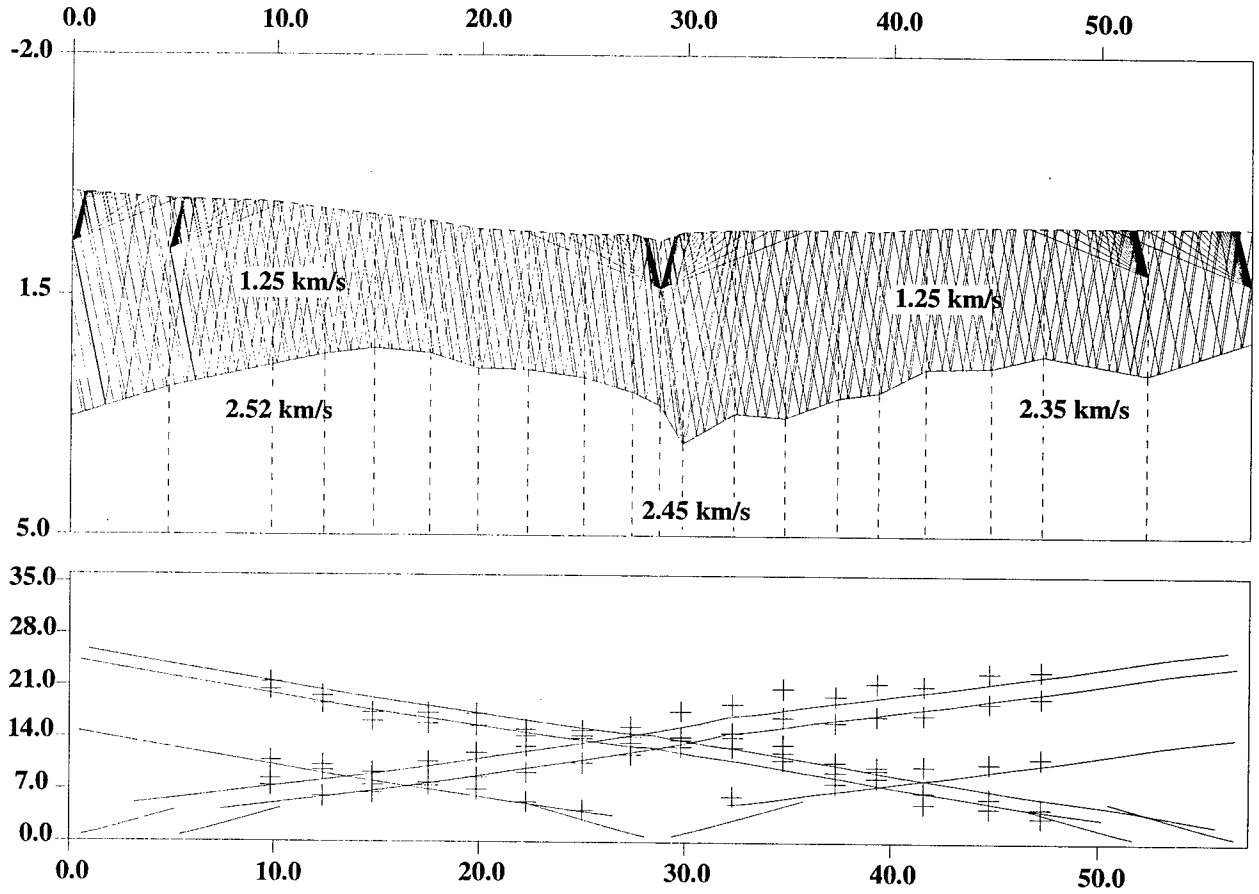

Site 9 RAYINVR

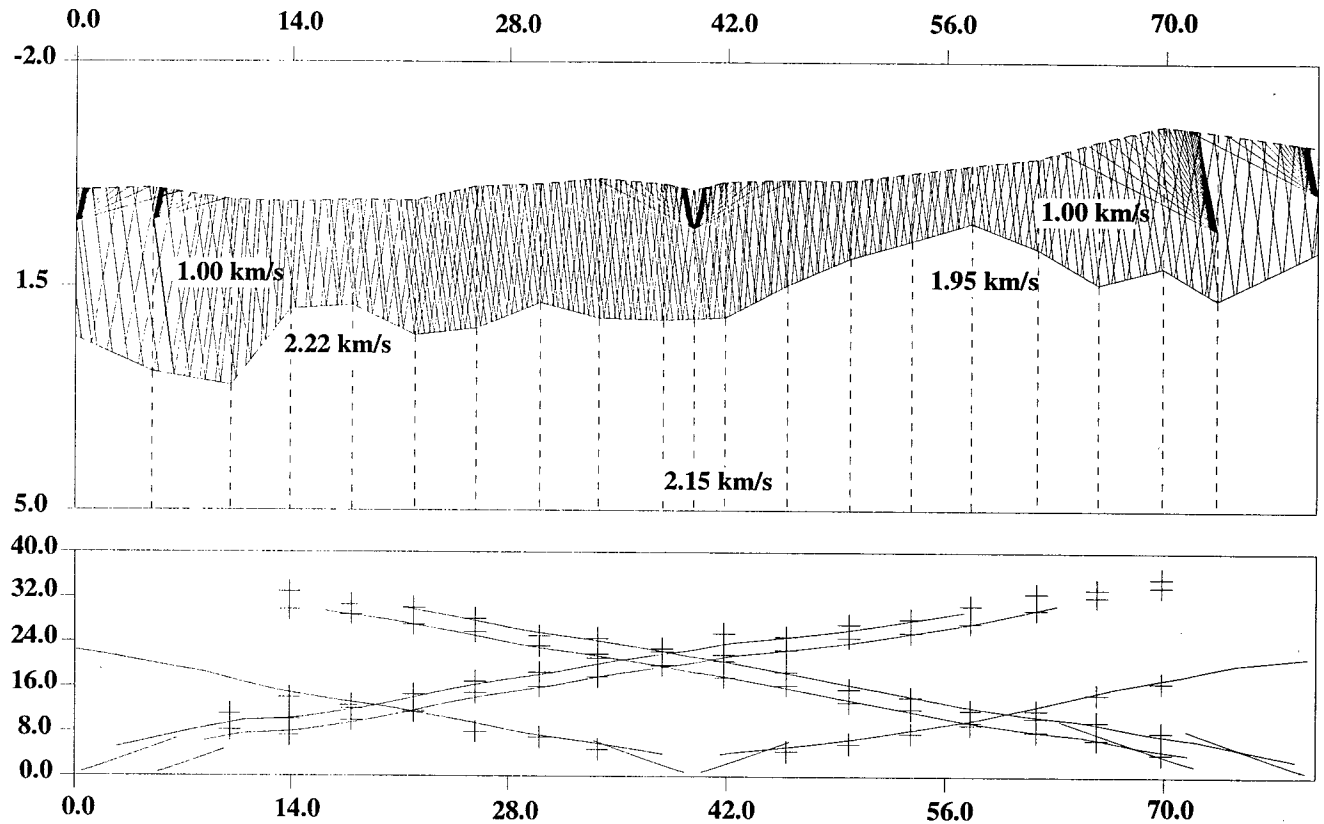

Site 10 RAYINVR

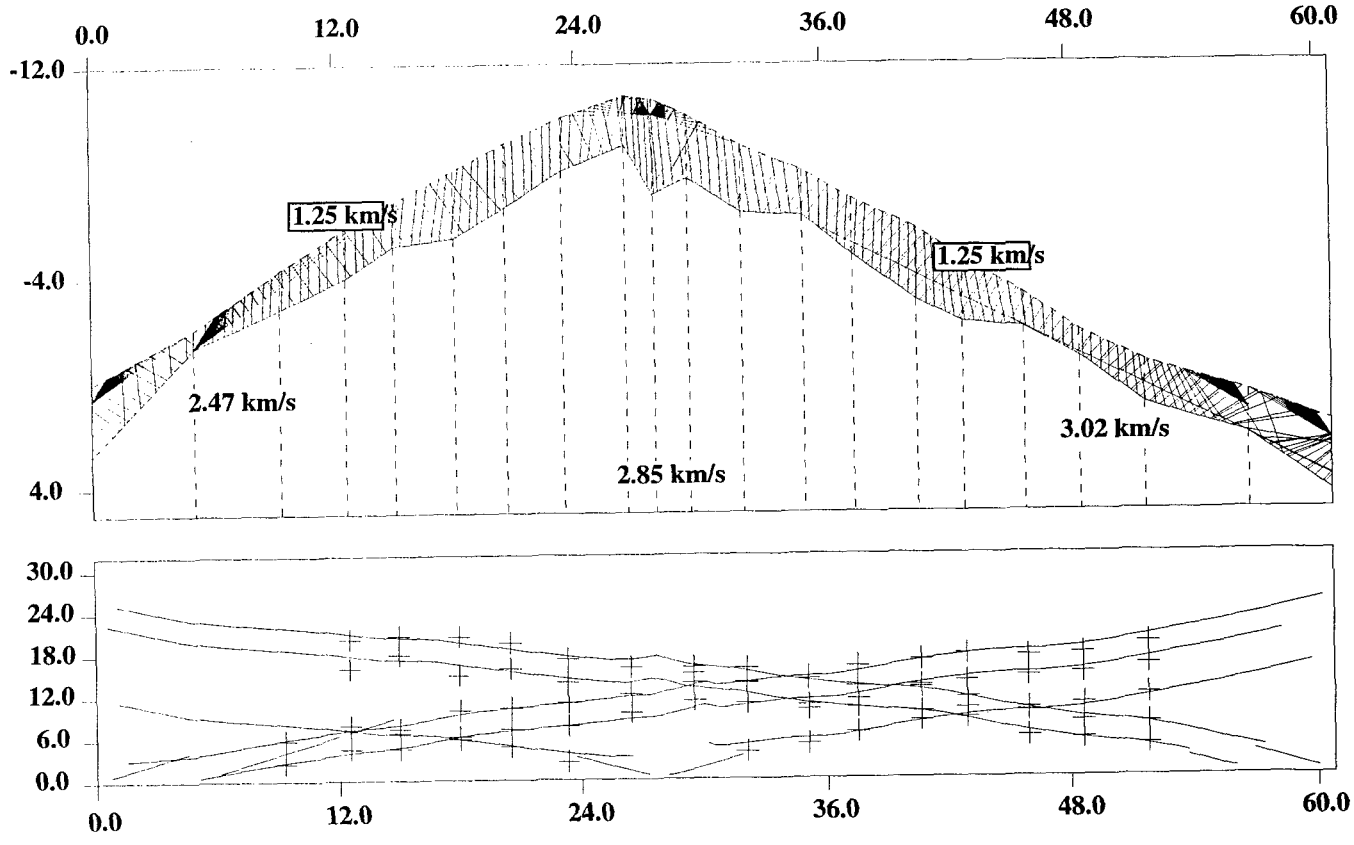

Site 11c RAYINVR

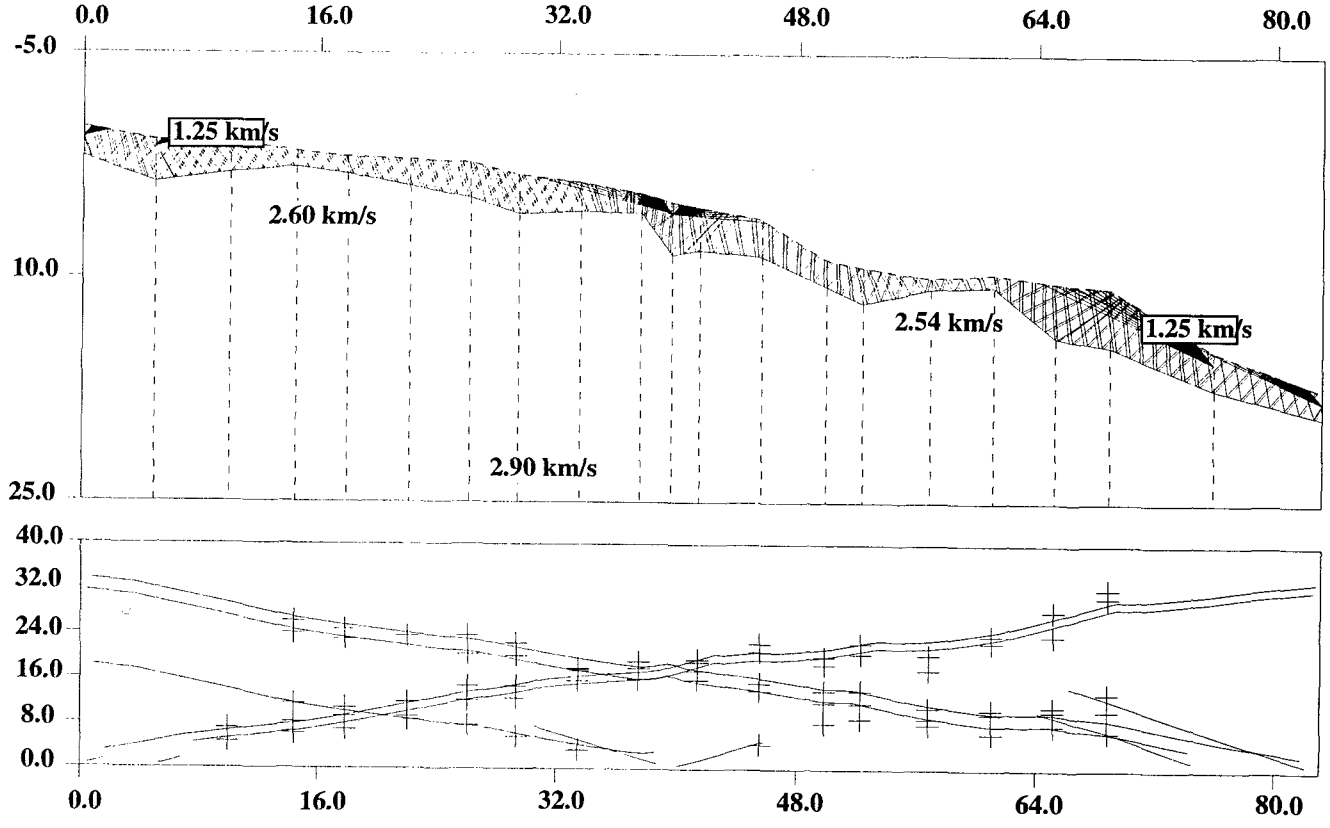

Site 11r RAYINVR

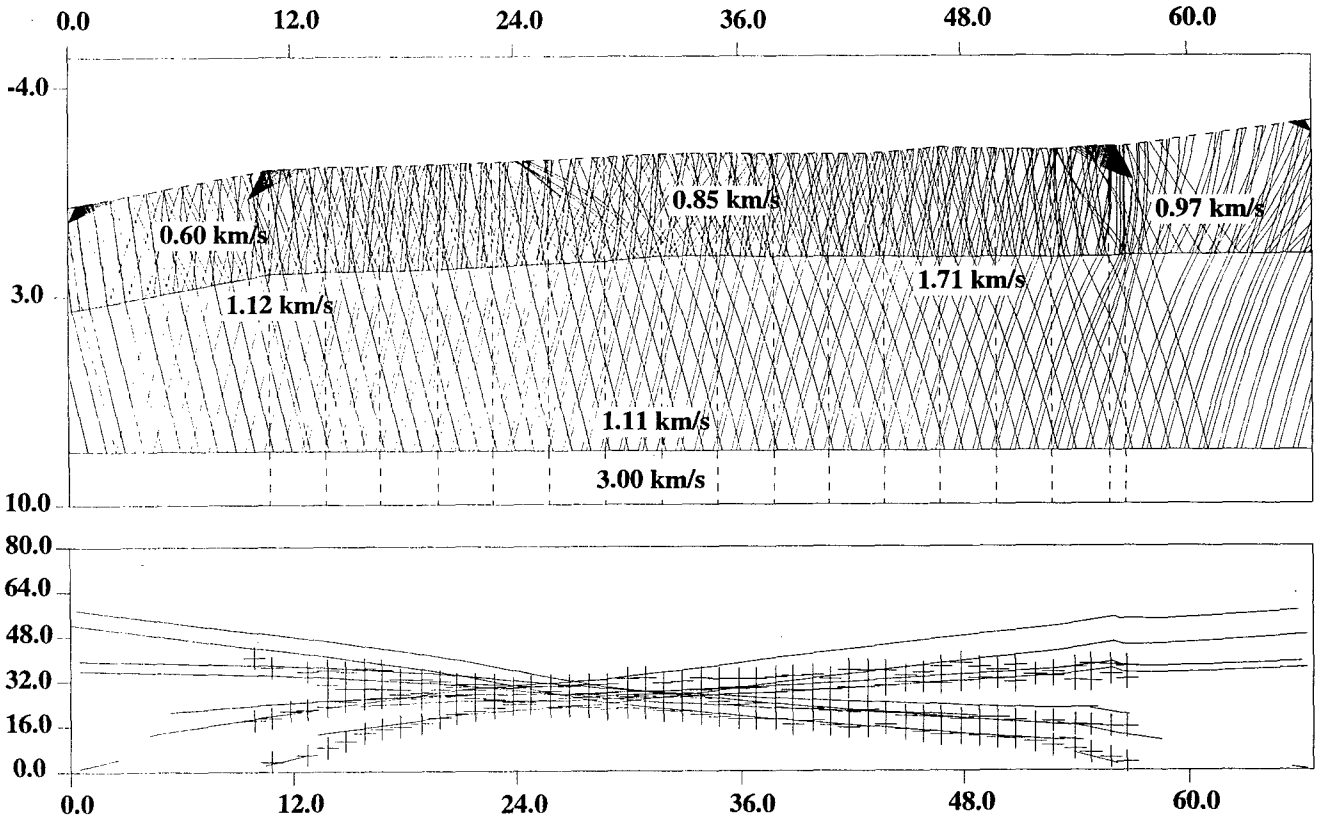

Site 12l RAYINVR

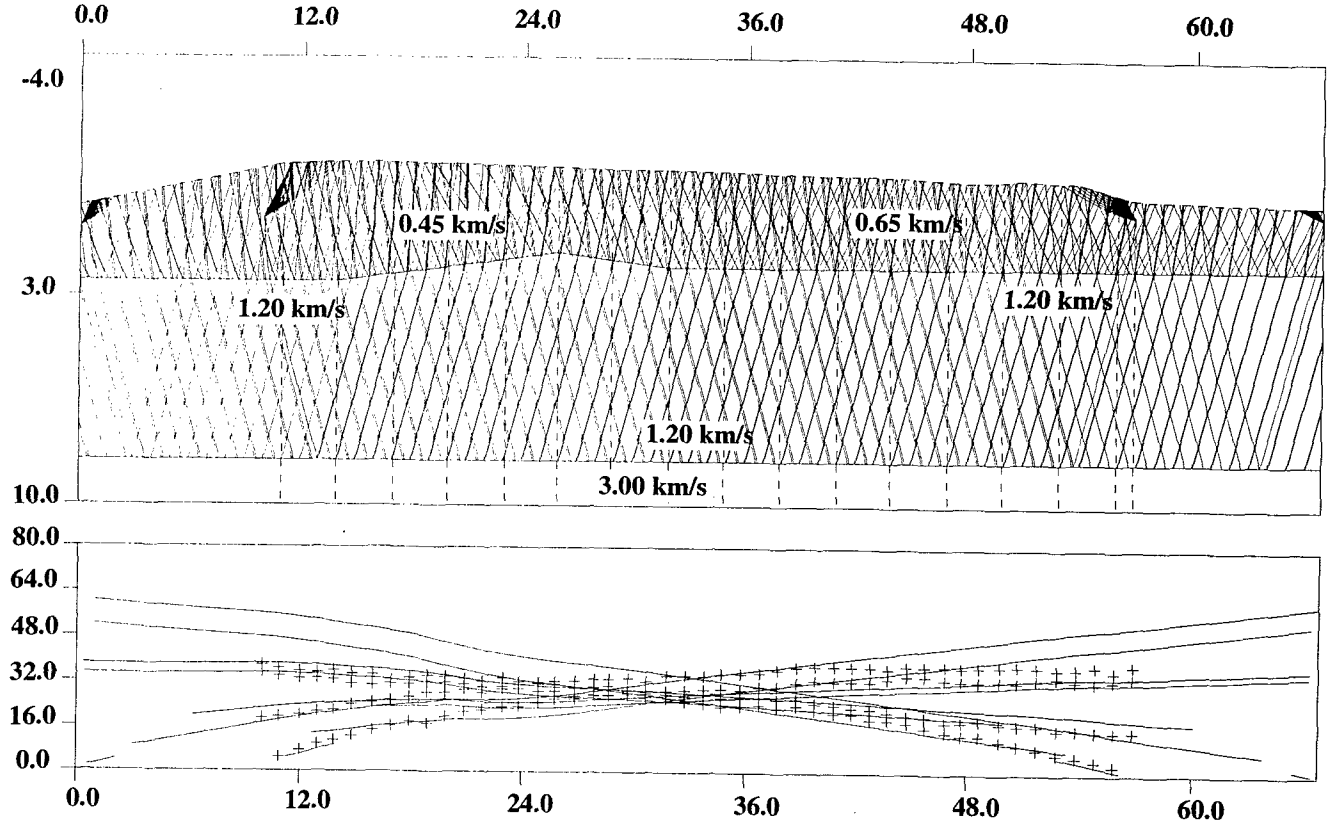

Site 12u RAYINVR